Final report on
LWS-FP wavelength calibration

S. Pezzuto

18 June 1998

1 Introduction

The LWS Fabry-Perot interforometers are fully described in Davies et al. (1995), but for this document, which explains the adopted strategy and the results of the wavelength calibration, we can simply think of a Fabry-Perot, hereinafter FP, as two partially transmitting mirrors facing each other a distance d apart.

Under simplifying assumptions the FP transmission has a maximum at wavelength λ when

$$\frac{\lambda m}{2} = d \tag{1}$$

where m is a positive integer called the order. Note that at separation d there are an infinity of transimitted wavelengths, namely $2d$, d, $2/3d$ and so on. To avoid contamination by undesired wavelengths LWS-FP used the grating as order sorter.

In Equation 1 there are no free parameters so that once d and m are known we can easily derive λ without needing a calibration. But the separation between mirrors was readout by the onboard electronics in terms of a quantity, the FP encoded position, whose relation with d is known from ground calibration to be a cubic function. So Equation 1 turns into

$$\frac{\lambda m}{2} = A + Bx + Cx^2 + Dx^3 \tag{2}$$

Being the result of a digital measurement, x is an integer running from 0 to 4095. Wavelength calibration means then to derive the 4 coefficients of the above polynomial.

2 Strategy of calibration

Let us assume that we have observed a number of lines at wavelengths λ_i and found their centres[1] x_i. We can not directly invert Equation 2 to find the unknown coefficients because we still miss the orders m_i. So that the first step is to observe the same line in at least two different orders, say m and $m+1$.

The AOT logic selected for each wavelength one single order, so to observe the same line at different orders the LIDT executed special dedicated observations (COIF). Once determined the centres x_1 and x_2 for the two orders we

[1]Note that the position of a centre, being the result of a fitting procedure, is no longer an integer but a decimal number.

recast Equation 2 in a different form

$$\frac{\lambda}{2} = B(x_2 - x_1) + C(x_2^2 - x_1^2) + D(x_2^3 - x_1^3)$$

After observing lines at different orders a first estimate of the coefficients is obtained with a least squares fit.

Now we rewrite Equation 2 in the following way

$$m_{i,j} = \frac{2}{\lambda_i}(A + Bx_{i,j} + Cx_{i,j}^2 + Dx_{i,j}^3)$$

where i refers to a given wavelength observed at orders j. All the m's must be integer so that the value of A which minimizes the differences $\|m_{i,j} - \mathrm{INT}(m_{i,j})\|$ is looked for. Once A is found Equation 2 is used to determine the orders m and finally all the four coefficients can be derived at the same time, again using a least squares fit.

This is the procedure used to derive the coefficients used in version 7 of the pipeline. As said, this approach is necessary because a priori we do not know the order at which a line has been observed. It is possible that future calibrations will be done following a different approach because when orders are already known the coefficients can be derived directly from Equation 2.

2.1 The line fitting algorithms

To find the centre of a line three algorithms have been used which are now briefly described. They have been implemented in IDL and the full procedures can be found in a separate document.

The three techniques are completely independent each other and give us a better estimate of the centre position and its error, defined as $\max\|x_i - \overline{x}\|$ with $\overline{x}$ the average of the three values x_i.

However the present calibration has been carried out according to the procedure described in the previous section which is part of the `CALIBAN` package (see CFPD document) and using only the first method (the centroid of the line). The three techniques have been used altogether during the monitoring program discussed later.

2.1.1 The centroid

The background is estimated, and then subtracted, by fitting a low order polynomial, ≤ 3, to the ends of the FP scan, far from the line. The line profile is divided in a number of points, usually 10, avoiding the wings and the peak where the profile could be distorted, e.g. by memory effects.

At each point the segment that intersects the line is found and the half point computed. The 10 half points are then averaged. The procedure, fully described in the LWS Calibration File Derivation Procedure, gives as output:

- the peak position and its error;
- the peak flus in term of photocurrent;
- the full width at half maximum (FWHM).

FP wavelength calibration

Source	Rev.	Line	Orders	
NGC 7027	168	[OI] 63.2	87, 88	
G 36.3 +0.7	300	[OIII] 51.8	104, 105, 106	
G 0.6 -0.6	321	[OIII] 51.8	105, 106	
NGC 7027	370	[OI] 63.2	88, 89	FPS
NGC 7027	175	[OI] 145.5	69, 70	
G 0.6 -0.6	287	[OIII] 88.4	114, 115	
G 36.3 +0.7	300	[OIII] 88.4	114, 115	FPL

Table 1: Lines and sources used to calibrate FP's. Rev. is the revolution number, wavelengths are in micron.

2.1.2 Fourier interpolation

The background is estimated as in the previous method. The line is then Fourier transformed and all the high frequencies filtered out. After an inverse transform the so smoothed line profile is reconstructed to find peak position and intensity as well as the FWHM.

2.1.3 Gaussian fitting

The IDL procedure `GAUSSFIT` has been used. It fits at same time background and line profile so from this point of view it is the best of the three methods presented. The procedure gives line centre, peak height and FWHM. Anyway FP line profile is definitively not Gaussian, being the convolution of the source intrinsic profile and an Airy function so that only the centre position is reliable.

Experience has shown that even at low signal to noise ratio, the three line centres seldom differ by more than 1 FP encoded position.

3 Calibration for version 7 of pipeline

Results of calibration for both FP's are accurately described by Swinyard (1997) so that here they are only briefly summarized.

Lines and sources observed for the short wavelenght FP (shortly FPS, used from 46.764 μ to 71.892 μ) and for the long wavelenght FP (shortly FPL, used from 70.186 μ to 197.094 μ) are reported in Table 1. The derived coefficients are written in Table 2.

	FPS	FPL
A=	2713.2569	5010.6224
B=	0.023870650	0.031654363
C=	$4.1581366 \cdot 10^{-7}$	$7.3574580 \cdot 10^{-8}$
D=	$-2.4636391 \cdot 10^{-11}$	$5.1097999 \cdot 10^{-11}$

Table 2: FPS (on the left) and FPL (on the right) wavelength calibration coefficients.

Lines and sources used to monitor FP's calibration

Line	Ion	FP	Source
51	[OIII]	S	G 0.6 -0.6, G 36.3 -0.7, NGC 7027, NGC 7538
57	[NIII]	S	NGC 3603, G 0.6 -0.6, NGC 6302
63	[OI]	S	NGC 7023, NGC 7027, NGC 7538, S 106
88	[OIII]	L	G 0.6 -0.6, G 36.3 -0.7, NGC 3603, NGC 7538
122	[NII]	L	G 0.6 -0.6
146	[OI]	L	NGC 7023, NGC 7027
158	[CII]	L	G 0.6 -0.6, NGC 6302, NGC 7023, NGC 7027, NGC 7538, S 106

Table 3: For each line they are reported: the ionic (or atomic) species, the FP used and the source.

4 Monitoring the calibration

To check the stability of the calibration against possible temporal trends, weekly observations have been performed on a number of selected sources, chosen according to their luminosity, visibility and with as small FWHM as possible. Lines and sources used for this task are reported in Table 3.

Each line has been fitted with the methods previously described so that its centre is the average of three values. It has been converted into wavelength using Equation 2 and by taking into account the relative motion of the source with respect to the satellite (see Appendix).

4.1 Results for FPS

In Figure 1 three plots are shown, one for each observed line. The calibration looks stable with no temporal trend. Note the [NIII] line has not been used to derive the calibration coefficients, so that we can use our data to measure its rest wavelength. Combining all the 11 measurements we get $\lambda \pm 1\sigma = 57.32952 \pm 0.00072\ \mu$, in perfect agreement with the quoted value in literature ($57.33\ \mu$). In Table 4 the RMS error for each wavelength is reported.

4.2 Results for FPL

For FPL the data from the monitoring program are plotted in Figure 2. It is clear that the calibration is not as good as in the case of FPS, being affected by

FPS RMS calibration errors

Line	Error	
	$10^{-4}\ \mu$	Km/s
[OIII] 51.8	9.5	5.5
[NIII] 57.3	7.2	3.8
[OI] 63.2	8.7	4.1

Table 4: RMS errors for each line observed as part of our monitoring program for FPS.

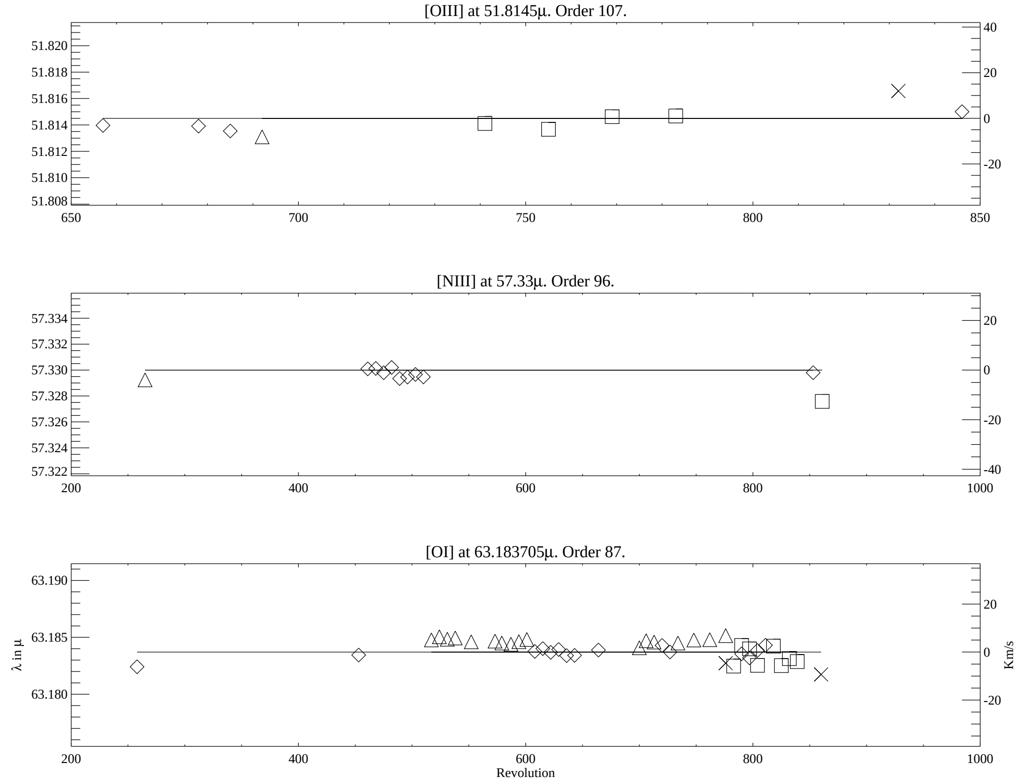

Figure 1: Monitoring data for FPS. Solid line: rest wavelength. Left ordinate: wavelength in micron; right ordinate: difference from rest wavelength in Km/s. Symbols: $\Diamond$ G 0.6-0.6 (top and middle plot), NGC 7023 (bottom plot); $\triangle$ G 36.3-0.7 (top), NGC 3603 (middle), NGC 7027 (bottom); $\Box$ NGC 7027 (top), NGC 6302 (middle), NGC 7538 (bottom); $\times$ NGC 7538 (top), S 106 (bottom).

FPL RMS calibration errors

Line		Error	
		10^{-3} μ	Km/s
[OIII]	88.4	1.5	5.1
[NII]	121.9	2.2	5.4
[OI]	145.5	6.6	13.6
[CII]	157.7	3.0	5.6

Table 5: RMS errors for each line observed as part of our monitoring program for FPL.

systematic errors. But even in the worst case (the [OI] line at 145.5 μ) errors are lower than half spectral resolution element. RMS errors are reported in Table 5. Note that when the measured wavelength is systematically shifted respect to the rest wavelength, the RMS is a measure of the average displacement and not a true scatter around the mean.

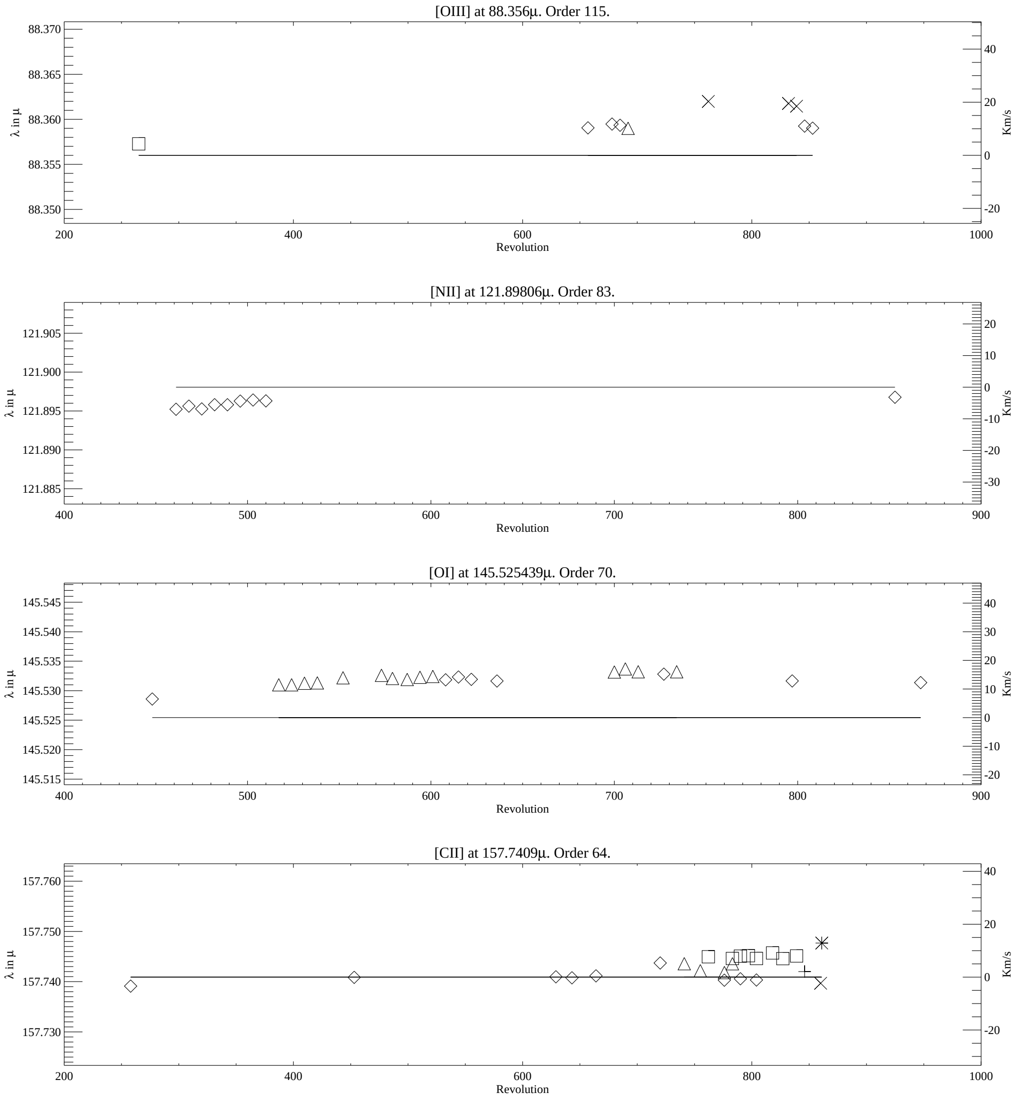

Figure 2: Monitoring data for FPS. Solid line: rest wavelength. Left ordinate: wavelength in micron; right ordinate: difference from rest wavelength in Km/s. Symbols: $\Diamond$ G 0.6-0.6 (first two plots), NGC 7023 (second two plots); $\triangle$ G 36.3-0.7 (first), NGC 7027 (third and fourth); $\square$ NGC 3603 (top), NGC 7538 (last); $\times$ NGC 7538 (first), S 106 (last); for the last plot $+$ G 0.6-0.6 and $*$ NGC 6302.

5 Wavelength accuracy

As is clear from Equation 1 or 2, the distance d was directly measured and not the wavelength λ. For this reason the accuracy on the calibration depends on which FP position range was used to observe a given line. This information is written in `LSPD` files.

In Figure 3 the relation between FPS encoded position and gap between plates is shown as a solid line. Asterisks mark the positions where a particular combination (λ, m) falls. The combinations actually selected by the AOT logic

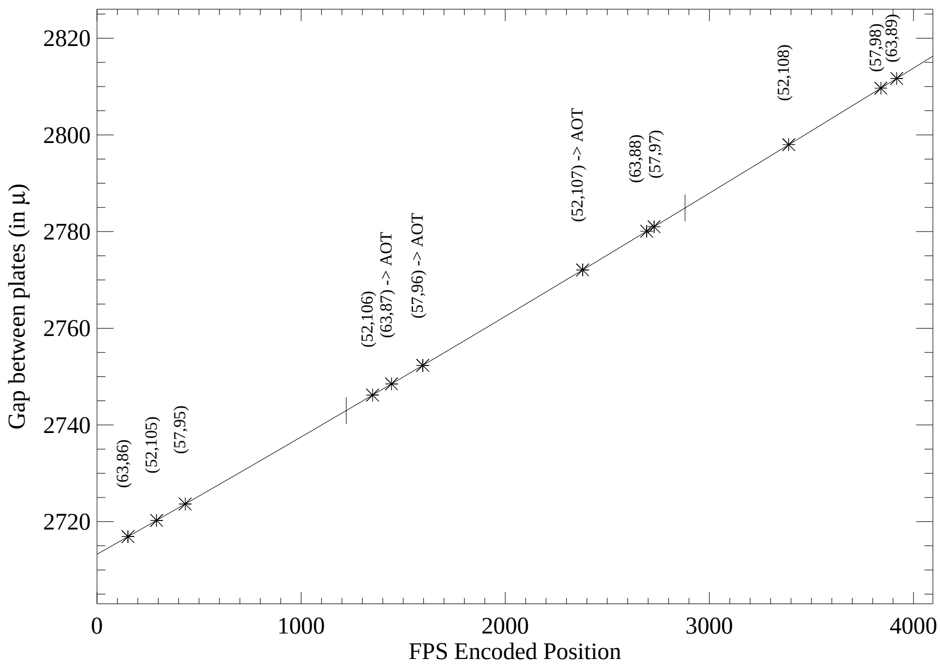

Figure 3: Distance between plates versus encoded position according to FPS wavelength calibration coefficients. The instrument has always been operated in the range delimited by the two small vertical segments. The asterisks mark the position corresponding to a particular combination (wavelength,order). To calibrate the instrument some other combinations have been used, also shown in the figure.

are indicated. All wavelengths observable with FPS correspond to a particular position inside the portion of the curve delimited by two vertical segments.

Looking at both Figure 3 and Table 4 we conclude that the accuracy of wavelength calibration is ~ 4 Km/s at positions $x < 2000$, slightly increasing to ~ 6 Km/s at greater x. A reasonable choice for error over the all range of positions is then $\Delta\lambda = 2.00 \cdot 10^{-5}\lambda$.

The analogous plot for FPL is in Figure 4. In this case the range swept by the instrument is larger than in the previous case. From this figure and Table 5 it is evident that a systematic error is present in the calibration, increasing toward larger x values. The origin of this shift is under investigation[2]. As of now we suggest to adopt for the final accuracy the most conservative value, i.e. half of the spectral resolution element (for the 146 μ line this corresponds to about $8 \cdot 10^{-3}$ μ), even if the internal scatter of data points, see Figure 2, seem to imply that a better accuracy could be reach in the future.

References

LWS Calibration File Derivation Procedures, LIDT (ed.) 1996. Document

[2] As discussed in the Appendix, there is some indication from FPS observations that the rest wavelength for the 88 μ line, used for FPL calibration, could be wrong.

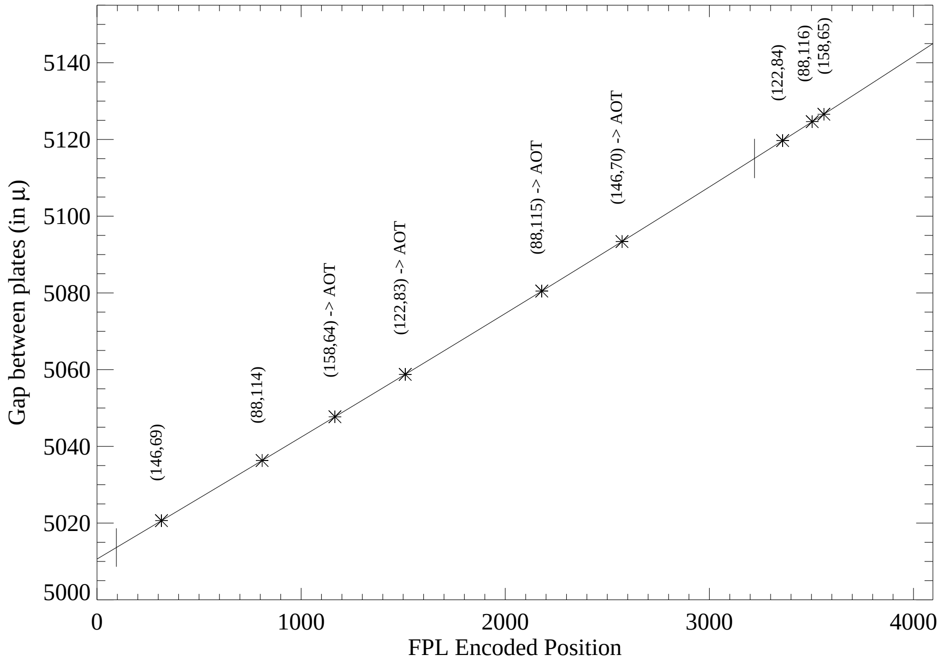

Figure 4: Same as the previous figure but for FPL. Note the larger interval of positions used.

LWS/IDT/N/0019.3 [CFPD]

Davis G. et al., 1995, Appl. Optics, 34, 92

Kerr F.J. & Lynden-Bell D., 1986, MNRAS, 221, 1023

Lockman F.J., 1989, ApJS, 71, 469

McGee R.X. & Newton L.M., 1981, MNRAS, 196, 889

Rogers C., Heyer M.H. & Dewdney P.E., 1995, ApJ, 442, 694

Schneider S.E., Terzian Y., Purgathofer, A. & Perinotto, M., 1983, ApJS, 52, 399

Shaver P.A., McGee R.X., Newton L.M., Danks A.C. & Pottasch S.R., 1983, MNRAS, 204, 53

Swinyard B., 1997. Document LWS/RAL/N/2883.01

A Input data

In the body of this document we were concerned with the right hand side of Equation 2, i.e. how to derive the unknown coefficients and to assess their accuracy. In this appendix we are going to discuss the left hand side of the equation, namely what number we have to substitute for λ.

Rest wavelengths	
Species	λ
[OIII]	51.8145
[NIII]	57.33
[OI]	63.183705
[OIII]	88.356
[NII]	121.897570
[OI]	145.525439
[CII]	157.7409

Table 6: The adopted rest wavelengths, in micron, for calibration/monitoring of LWS-FP.

If $\lambda_{\rm r}$ is the rest, or vacuum, wavelength, the Doppler correction is

$$\lambda = \lambda_{\rm r} \frac{\sqrt{1 - V_{\rm Tot}^2/c^2}}{1 - V_{\rm Tot}/c} \tag{3}$$

where $V_{\rm Tot}$ is the relative velocity of ISO with respect to the source, and c the velocity of light (adopted value $2.99792 \cdot 10^5$ Km/s).

In Table 6 the rest wavelengths used for calibration and monitoring are reported. They have been taken from the WEB at the following URL addresses:

- `http://www.mpe-garching.mpg.de/ISO/linelists/index.html`
- `http://www.pa.uky.edu/~peter/line_list/linelist.html`

As written in Section 4.1, for the present calibration the 57 μ line has not been used so that our data can be considered as an independent measurement of the line whose rest wavelength results $\lambda \pm 1\sigma = 57.32952 \pm 0.00072\ \mu$. The 88 μ line has been observed also with FPS whose accuracy, as previously described, is very good. This line, at order 62, falls at positions around 1000 and around 2800 at order 63. Using only the observations at order 62, where higher is the accuracy of FPS, and with high signal to noise ratio the rest wavelength we derived is $\lambda \pm 1\sigma = 88.36017 \pm 0.00036\ \mu$. Using all the FPS observations the value does not change significantly but the error increases. The details of this measurement are in Table 7.

Measurement of [OIII] wavelength

Rev	Pos	Source	Rest λ
093	1072.06	NGC 3603 P1	88.360119
650	1078.67	G 0.6-0.6	88.359844
671	1079.84	G 0.6-0.6	88.360565

Table 7: Data relative to the three FPS [OIII] line observations used to measure the rest wavelength. Rev: revolution, Pos: line centre in FPS encoded position, Source: source name, Rest λ: measured wavelength after taking into account satellite motion.

Dynamical data for observed sources

Source	$V_{\rm LSR}$	Ref	$V_{\rm Sun}$	(l, b)	
NGC 3603	+17.8	(1)	−10.7012	291.63	−0.53
GRS 000.60 -00.60	+16.6	(2)	+10.0663	0.57	−0.63
[L89b] 36.289 +00.734	+76.5	(3)	+17.2731	36.29	0.73
NGC 7023	+3.7	(4)	+14.0618	103.99	+14.27
NGC 7027	+24.0	(5)	+15.7170	84.93	−3.50
NGC 7538	−60.8	(3)	+10.7582	111.54	0.78
NGC 6302	−31.4	(5)	+7.1722	349.51	1.06
[L89b] 76.383 −0.623	+4.0	(3)	+17.2363	76.38	−0.62

Table 8: For each source it is here reported: the name, as used in SIMBAD database (note that in the text the two [L89b] objects are referred to as G36+0.7 and S 106 respectively), the velocity with respect to Local Standard of Rest and its reference, the velocity of the Sun with respect to LSR projected to the source and the Galactic coordinates as given by SIMBAD. References are as follows: (1) McGee & Newton (1981); (2) Shaver et al. (1983); (3) Lockman (1989); (4) Rogers et al. (1995); (5) Schneider et al. (1983).

For the velocity we have

$$V_{\rm Tot} = V_{\rm LSR} - V_{\rm Sun} - V_{\rm ISO} \tag{4}$$

The last addendum in the right hand side, $V_{\rm ISO}$, is actually the sum of the satellite velocity around the Earth, and the Earth velocity around the Sun. It depends on satellite orbital motion and it is written in the header of `LSAN` files at three reference times (keywords `TREFDOP`i, with $i = 1, 2, 3$) corresponding more or less at the beginning, middle and end of the observation. We used the average of these 3 values, which differs each other of a few 10^2 m/s.

$V_{\rm Sun}$ is the velocity of the Sun with respect to the Local Standard of Rest (LSR), projected toward the source. It can vary by a few Km/s according to the different definition of LSR, for this work we used the values reported in Kerr & Lynden-Bell (1986): $u = 10.0$, $v = 15.4$ and $w = 7.8$ Km/s in the velocity space defined by the Galactic plane and the axis perpendicular to it. If (l, b) are the Galactic coordinates of a generic source the projection is given by the usual formula

$$V_{\rm Sun} = u \cos l \cos b + v \sin l \cos b + w \sin b \tag{5}$$

In Table 8 the reader can find the $V_{\rm LSR}$, $V_{\rm Sun}$ and (l, b), for each observed source.